Petroleum Science 20 (2023) 3887–3896

Contents lists available at ScienceDirect

Petroleum Science

journal homepage: www.keaipublishing.com/en/journals/petroleum-science

Original Paper

Study on the in situ desulfurization and viscosity reduction of heavy oil over MoO_3–ZrO_2/HZSM-5 catalyst

Rui-Qi Liu, Li-Qiang Zhang, Hui-Da Pan, Yi-Ya Wang, Jin-Yu Li, Xin-Wei Wang, Zheng-Da Yang, Xin-Lu Han, Ri-Yi Lin*

College of New Energy, Qingdao Engineering Research Center of Efficient and Clean Utilization of Fossil Energy, China University of Petroleum (East China), Qingdao, 266580, Shandong, China

ARTICLE INFO

Article history:
Received 12 July 2022
Received in revised form
8 March 2023
Accepted 7 August 2023
Available online 7 August 2023

Edited by Jia-Jia Fei

Keywords:
Heavy oil
Hydrothermal cracking
MoO_3–ZrO_2/HZSM-5 catalyst
Desulfurization
Viscosity reduction

ABSTRACT

Heavy oil is characterized by high viscosity. High viscosity makes it challenging to recover and transport. HZSM-5, MoO_3/HZSM-5, ZrO_2/HZSM-5 and MoO_3–ZrO_2/HZSM-5 catalysts were developed to promote in situ desulfurization and viscosity reduction of heavy oil. The physical and chemical properties of catalysts were characterized by XPS, XRD, TEM, NH_3-TPD, etc. The effects of temperature, catalyst type and addition amount on viscosity and composition of heavy oil were evaluated. The results showed that the presence of MoO_3–ZrO_2/HZSM-5 nanoparticles during aquathermolysis could improve the oil quality by reducing the heavy fractions. It reduced viscosity by 82.56% after the reaction at 280 °C and catalyst addition of 1 wt%. The contents of resins and asphaltic in the oil samples were 5.69% lower than that in the crude oil. Sulfur content decreased from 1.45% to 1.03%. The concentration of H_2S produced by the reaction was 2225 ppm. The contents of sulfur-containing functional groups sulfoxide and sulfone sulfur in the oil samples decreased by 19.92% after the catalytic reaction. The content of stable thiophene sulfur increased by 5.71%. This study provided a basis for understanding the mechanism of heavy oil desulfurization and viscosity reduction.

1. Introduction

Oil will remain the primary source of energy over the next 20 years (Ghanavati et al., 2013; Sitnov et al., 2018). Heavy oil accounts for 70% of the remaining oil reserves in the world (Parejas et al., 2021). However, heavy oil is characterized by high viscosity, high density, and poor fluidity. This causes significant difficulties in exploiting and transporting heavy oil (Hart, 2013; Liu et al., 2020; Taborda et al., 2017; Muraza and Galadima, 2015; de Klerk, 2021).

Heavy oil has a high content of resins and asphaltic (Antwi Peprah et al., 2023). Resins and asphaltic molecules have a strong interaction. They combine and aggregate into macromolecular aggregates that increase the viscosity of heavy oil (Lv et al., 2019; Headen et al., 2017; Groenzin and Mullins, 2000). Clark et al. (1988) proposed the concept of hydrothermal cracking reaction. The viscosity reduction is caused by the hydrothermal cracking reaction in the thermal recovery process (Dutta et al., 2000). The C–S bond is broken by the hydrothermal cracking reaction (Clark and Kirk, 1994). The heavy component is decomposed into light components (Lin et al., 2020). Therefore, the viscosity of heavy oil decreases.

Weissman (1997) proposed that catalysts promote desulfurization and viscosity reduction in heavy oil during the in situ upgrade. This has facilitated the development of viscosity reduction research in heavy oil. In the oil reservoir environment (certain temperature, pressure and water content), catalysts can promote the fracture of chemical bonds in heavy oil (Wang et al., 2021). Therefore, the development of efficient catalysts is essential for the utilization of heavy oil resources (Schuler et al., 2015; Hofko et al., 2015; Zhao et al., 2016). Nanocatalysts have high specific surface area, strong surface adsorption and amphiphilicity (Hashemi et al., 2013). Nanoparticles are considered promising catalysts for enhanced oil recovery (Lin et al., 2019; Hendraningrat and Torsæter, 2014; Li et al., 2016; Lakhova et al., 2017). It proves nanoparticles are easier to enter macromolecules in fluids and react with internal chemical bonds to reduce the viscosity (Li et al., 2022). Montoya

* Corresponding author.
E-mail address: linry@upc.edu.cn (R.-Y. Lin).

https://doi.org/10.1016/j.petsci.2023.08.005

et al. (2016) proposed that bimetallic nanoparticles exhibit better catalytic properties than monometallic nanoparticles. In addition, some scholars also study the mechanism of catalytic hydrothermal cracking of heavy oil. They point out that groups containing heteroatoms (N, O, and S) in heavy oil can cause aggregation and form hydrogen bonds. Thus, heavy oil has high viscosity (Chen et al., 2009a). Almost all the studies support the mechanism that catalyzes the C–S bond cleavage. This is the main reason why the viscosity of heavy oil eventually decreases.

However, the catalysts have a narrow activity temperature window. A large amount of coke is generated above 300 °C. It affects the viscosity reduction effect (Sviridenko et al., 2020; Safaei Mahmoudabadi et al., 2021). At low temperatures, most catalysts do not have sufficient contact with heavy oil, and the viscosity reduction effect is also poor (Suwaid et al., 2020). Therefore, it is necessary to develop a catalyst with a wide temperature window (Baharudin et al., 2019; Kordulis et al., 2016; Dutta et al., 2000). Zeolite is an excellent catalytic material (Zaykovskaya et al., 2020). It is crystalline aluminosilicate material composed of tetrahedrons of AlO_4 and SiO_4 connected with oxygen atoms. Due to the structural shape selectivity of micropores, they are widely used as catalysts (Jong et al., 2010; Ghanbari et al., 2018; Aghaei and Haghighi, 2014; Dong et al., 2009). HZSM-5 is a zeolite molecular sieve catalyst that has been widely used. It has high thermal stability, acid resistance, hydrophobicity and good carbon deposition resistance. Transition metals are excellent catalysts for catalytic hydrogenation (Antwi Peprah et al., 2020). Wang et al. (2012) prepared WO_3/ZrO_2 catalysts. WO_3 is uniformly dispersed on ZrO_2. Mo catalysts have good hydrogenation activity and coke inhibition (Hart et al., 2015). Olvera et al. (2014) used NiMoWC catalyst, and the viscosity reduction rate reached 97%.

Therefore, in this work, HZSM-5-based nanocatalysts were prepared and analyzed. Next, some experiments were conducted and analyzed, including the effects of temperature, catalyst type and addition amount on the viscosity of heavy oil. Finally, the viscosity reduction and desulfurization mechanisms were discussed in detail.

2. Experimental

2.1. Preparation of catalysts

Fig. 1 shows the catalyst preparation process. The catalyst was prepared by excessive impregnation. The ion exchange resin was not used. The metal oxides are only loaded on the surface of the molecular sieve. A 1 mol/L solution of zirconium nitrate pentahydrate ($Zr(NO_3)_4 \cdot 5H_2O$) (McLean Reagent Co., Ltd., China) and 1 mol/L solution of ammonium molybdate ($(NH_4)_2MoO_4$) (McLean Reagent Co., LTD., China) were prepared. The HZSM-5 molecular sieve was impregnated in the configured solution. The water bath was heated in the ultrasonic oscillator until the excess water was dried. The obtained solids were dried in an oven at 80 °C for 24 h. The prepared solid powder was roasted in a muffle furnace at 500 °C for 6 h for activation. After cooling to room temperature, the activated catalyst was ground and screened to a particle size below 40–50 mesh.

2.2. Characterization of catalysts

X-ray diffraction (XRD) was performed on an X' Pert Philips diffractometer with Cu-Kα radiation. Operating conditions: Cu-Kα line ($\lambda = 0.154$ nm), scanning range of 5°~75°, tube pressure 40 kW, tube flow 40 mA, scanning speed 5 °/min, step size 0.02°. Brunauer-Emmett-Teller (BET) specific surface areas (SSAs) of the catalysts were measured by automated surface area and pore size analyzer (Micromeritics ASAP2460). The samples were desorbed under a nitrogen atmosphere at 300 °C for 4 h. The experimental data was calculated and processed by the BET algorithm. The morphology of the samples was characterized by a JEM-2100UHR transmission electron microscope (TEM). The maximum acceleration voltage of TEM was 200 kV, the point resolution was 0.19 nm, and the line resolution was 0.14 nm. Temperature-programmed desorption test of NH_3 (NH_3-TPD) was carried out by AutoChem II 2920 chemisorption instrument. The temperature was heated to 300 °C for 2 h at 10 °C/min in the He atmosphere, then dropped to 70 °C. 5% NH_3–He mixture was adsorbed for 30 min. After the baseline was stabilized, the temperature was heated to 800 °C at 10 °C/min. The desorption curve was recorded. The valence states of O, Al, Mo, Zr, and Si in the catalyst were analyzed by X-ray photoelectron spectroscopy (XPS). The parameters were set to excitation light source MgK (1254 eV), power 250 W and energy 35.75 eV. The active component loading of the catalyst was obtained by analysis and calculation.

2.3. Hydrothermal cracking experiment

Heavy crude oil from the Shengli Oilfield of China. The viscosity of the crude oil is 38200 mPa s at 50 °C. The experimental device is shown in Fig. 2. A typical experimental procedure was described: 30 g of heavy oil and 0.5 mL of hydrogen supply agent (1,2,3,4-tetrahydronaphthalene) were added into a 350 mL autoclave under different catalysts, catalyst addition amount, and reaction temperature conditions. The reaction time was 24 h. After the autoclave cooled to room temperature, the products were collected and tested for viscosity determination, hydrogen sulfide concentration, and SARA analysis.

2.4. Analysis of oil samples

The viscosity of heavy oil was recorded by the programmable viscosimeter (Brookfield DV-II+) at 50 °C. The torque was kept within a range of 20%–80% during measurement. The viscosity reduction rate (*VRR*) of heavy oil was calculated by the method below:

$$VRR = \frac{\eta_0 - \eta}{\eta_0}$$

where *VRR* , η_0, and η were viscosity reduction rate, viscosity before reduction, and viscosity after reaction, respectively. The experiments were carried out according to the method of bitumen separation of four components of NB/SH/T 0509–2010. The four components in the heavy crude oil samples were analyzed. Asphaltene was precipitated from crude oil by *n*-heptane. SARA separation was carried out in a column filled with alumina. Elementar Vario EL III carried out elemental composition analysis. The mass fraction of C, H, N, and S elements in the sample was determined. The mass fraction of the O element was obtained by the difference subtraction method. The reduction tube temperature was 550 °C. The carrier gas flow was 180 mL/min. The absolute error was less than 0.1%. X-ray photoelectron spectroscopy (XPS) was used to analyze the oil samples before and after the reaction.

3. Results and discussion

3.1. Characterization of catalysts

3.1.1. XRD analysis

The XRD power pattern of the catalyst was illustrated in Fig. 3. The characteristic diffraction spectrum lines of ZrO_2 at $2\theta = 30.2°$,

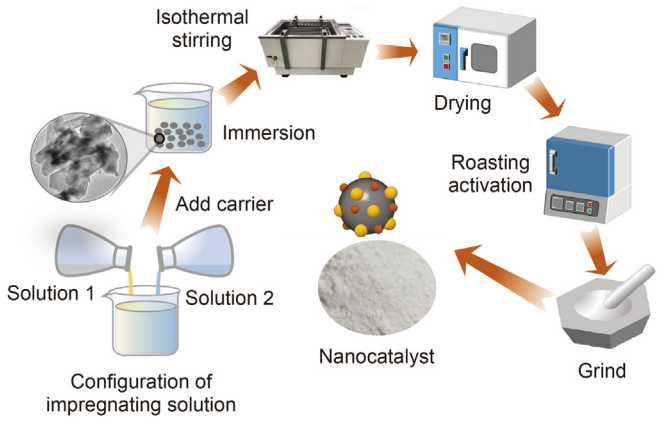

Fig. 1. The preparation process of catalysts.

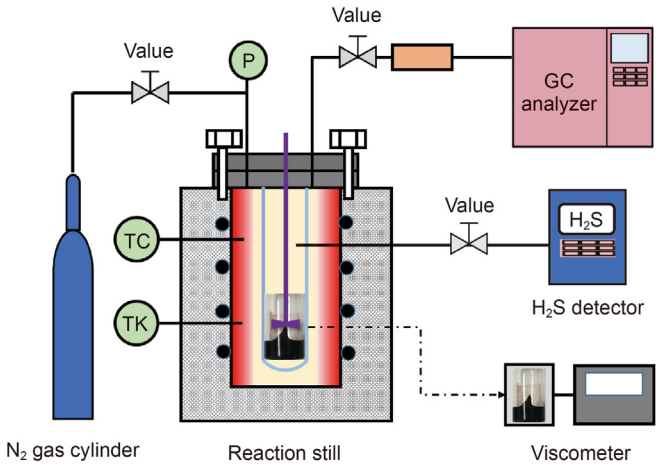

Fig. 2. Schematic diagram of the hydrothermal cracking reaction device.

35°, 50.5°and 60° were observed. The intensity and crystallinity of the characteristic diffraction peaks of molecular sieve decreased with the increase of ZrO_2 loading (Al-Attas et al., 2019; Avbenake et al., 2019). The characteristic diffraction spectrum lines of MoO_3/HZSM-5 at $2\theta = 25.7°$ and 38.9° were observed. A clear absorption peak of the supported catalyst could be seen by comparing the XRD patterns of the molecular sieve and the supported catalyst. The crystallinity of the molecular sieve decreased because of the load of ZrO_2 (Oh et al., 2020). The narrower diffraction peak of the active component indicated that the crystallinity of the MoO_3 loaded molecular sieve was higher. In addition, the diffraction peaks of the loaded molecular sieve $2\theta = 7.9°$, 8.8° and 23°–24° did not change significantly. This indicated that the loading of active components did not alter the mesoporous structure of the molecular sieve (Zhang et al., 2019; Laredo et al., 2004).

3.1.2. BET analysis

According to the test data in Fig. 4, the specific surface area of the molecular sieve decreased with the increase of active component loading. Because metal oxides were supported on the catalyst surface, the specific surface area of molecular sieves fell. The specific surface area of the catalysts loaded with 10 wt% ZrO_2 was higher than that of the molecular sieve. This may be due to adding a small amount of nitric acid solution during the configuration process, which increased the solubility of zirconium nitrate. The specific surface area of the molecular sieve increased. Because some

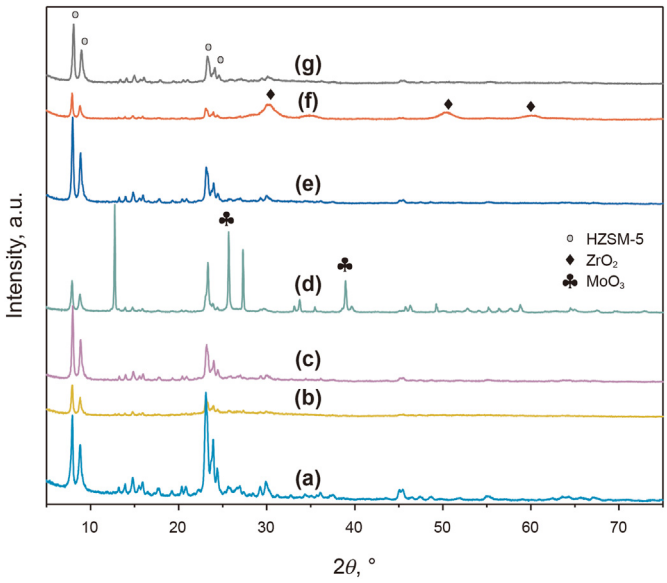

Fig. 3. XRD spectrum of the catalyst. (**a**): HZSM-5; (**b**): 10 wt% ZrO_2–MoO_3/HZSM-5; (**c**): 20 wt% ZrO_2–MoO_3/HZSM-5; (**d**): 10 wt% MoO_3/HZSM-5; (**e**): 20 wt% MoO_3/HZSM-5; (**f**): 10 wt% ZrO_2/HZSM-5; (**g**): 20 wt% ZrO_2/HZSM-5.

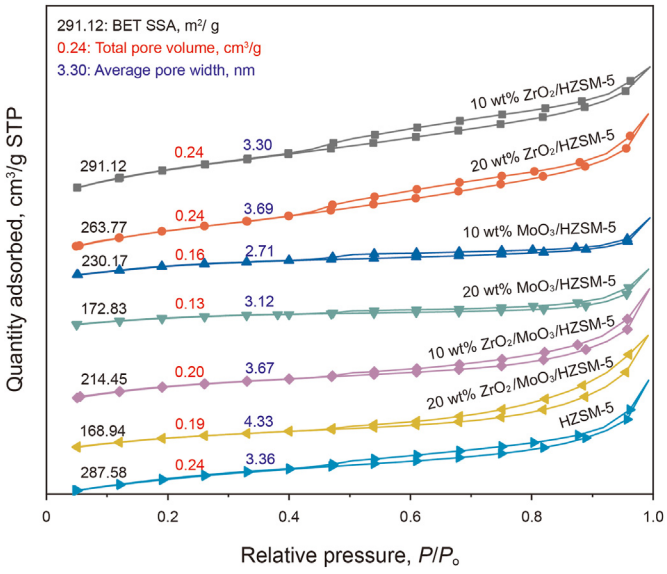

Fig. 4. Nitrogen adsorption and desorption isotherm.

nitric acids corroded the molecular sieve, the metal oxides did not fill the corrosion area (Nguyen et al., 2017; Wei et al., 2020). When the active metal loading increased to 20 wt%, the pore volume decreased with loading. This indicated that metal oxides were loaded into the pore channels of the molecular sieve, which reduced pore volume (Zhang et al., 2020). The average pore size of the molecular sieve increased because metal oxides blocked smaller pores and left larger pores. The asphaltene macromolecular structure in heavy oil is about 1 nm. It can freely enter the pores of the molecular sieve to participate in the reaction. In addition, the mesoporous structure could ensure the rapid discharge of reaction products and effectively reduce the generation and accumulation of carbon deposition (Liu et al., 2019; Muley et al., 2015; Mullins, 2010; Qiu et al., 2020). The nitrogen adsorption-desorption curve is shown in Fig. 4. The catalyst has a typical Langmuir II isothermal

curve and an H3 hysteresis ring. This indicated that the catalyst carrier was a mesoporous layered molecular sieve with narrow slits (Chen et al., 2009b; Hosseinpour et al., 2020).

3.1.3. TEM analysis

Fig. 5(a)–(c) showed TEM images of HZSM-5, ZrO_2/HZSM-5, and MoO_3/HZSM-5. It could be seen that the surface of the molecular sieve had distinct lattice stripes. The particles were well dispersed. Most particles appeared as short prismatical structures with an average diameter of around 30 nm. This proved that the ZrO_2/HZSM-5 and MoO_3/HZSM-5 catalysts were prepared as nanoparticles. The interplanar crystal distance of ZrO_2/HZSM-5 is 0.30 nm. The interplanar crystal distance of MoO_3/HZSM-5 is 0.23 nm (Li et al., 2017; Cui et al., 2020).

3.1.4. NH_3-TPD

It could be observed from Fig. 6 that NH_3 desorption peaks occur in all the prepared catalysts at about 160 and 420 °C. The desorption of NH_3 caused the low-temperature peak (160 °C) at the weak acid position. The high-temperature peak (>400 °C) was the desorption of NH_3 adsorbed on the strong acid position. In particular, the area of the NH_3 desorption peak could be used to measure the acidity of the molecular sieve. In general, the peak area of the low-temperature region in the desorption curve represented the number of weak acid sites, and the peak area of the high-temperature region represented the number of strong acid sites. The experimental results showed that the weak acid sites of the molecular sieve loaded with functional metal oxides decreased and the strong acid sites increased. The acid area of the molecular sieve loaded with ZrO_2 increased when the temperature was 600 °C. The acid area of the molecular sieve packed with MoO_3 increased to about 450 °C. Both loads increased the strongly acidic site of the catalyst (Li et al., 2019a, 2019b, 2020; Bandara et al., 2006; Tran et al., 2020; Hu et al., 2020).

3.1.5. XPS characterization

XPS characterized the content of metal elements loaded by the molecular sieve. The metal oxides were successfully loaded on the molecular sieve. The load was close to the expected value. There was a deviation in the load of some catalysts because of the uneven loading of catalysts. The results showed that when the content of MoO_3 exceeded 7–8 wt%, the MoO_3 could not continue to be loaded on the molecular sieve when the two metal oxides were mixed. However, the load of ZrO_2 could reach 17–18 wt%. This may be because the pores and surfaces of the molecular sieve were already loaded with active components (Yang et al., 2020).

The peaks of Mo and Zr were observed in survey spectra. The binding energies were calibrated by C 1s (284.8 eV). From the Mo 3*d* spectrum, the binding energies of Mo $3d_{3/2}$ and Mo $3d_{5/2}$ were 232.1 and 235.2 eV, respectively, which indicated that Mo ions present as Mo^{6+} on the surface of the nanoparticles. From the Zr 3*d* spectrum, the binding energies of Zr $3d_{3/2}$ and Zr $3d_{5/2}$ were 181.9 and 184.3 eV, respectively, which indicated that Zr ions presented as Zr^{4+} on the surface of the nanoparticles. These results also showed that the two active components existed in the form of MoO_3 and ZrO_2. Three peaks were located around 528.2–532.5, 529.0–532.5, and 530.5–533.2 eV in the XPS O *1s* spectrum. The peaks at 528.2–532.5 and 529.0–532.5 eV were assigned to the lattice oxygen atoms, chemically adsorbed oxygen and weakly bound oxygen. The peak at 530.5–533.2 eV was designated as the adsorbed water (Yenumala et al., 2020). The proportions of the three oxygen forms were 43.35%, 19.70% and 36.96%, respectively. It proved that lattice oxygen mainly exists on the catalyst.

3.2. Effect of different factors on desulfurization viscosity of heavy oil

3.2.1. Types of catalysts

The effects of different catalysts were shown in Fig. 7. HZSM-5, 10 wt% MoO_3–ZrO_2/HZSM-5, 20 wt% MoO_3–ZrO_2/HZSM-5, 20 wt % ZrO_2/HZSM-5 and 20 wt% MoO_3/HZSM-5 were used for catalytic experiments. After adding 20 wt% MoO_3–ZrO_2/HZSM-5 catalyst, the viscosity reduction rate of heavy oil was 83.94%. After adding 10 wt% MoO_3–ZrO_2/HZSM-5 catalyst, the heavy oil viscosity reduction rate was 82.56%. When the same amount of ZrO_2 or MoO_3 was loaded alone, the viscosity reduction rate was 67.15% and 63.75%, respectively. The catalytic viscosity reduction effect was lower than that of the catalysts supported by a mixture of two active metals.

Fig. 7 showed that under the catalytic action of 20 wt% ZrO_2/HZSM-5, H_2S gas produced the most in the reaction. This showed that it had the best desulfurization effect. However, ZrO_2 could not inhibit coke formation well. However, the coke production during hydrothermal cracking reaction would affect the decrease of oil viscosity, and ZrO_2 could not inhibit coke formation well. The MoO_3 has an inhibitory effect on coke formation. The promoting effect of MoO_3 on C–S bond fracture was less than ZrO_2. Therefore, the catalyst loaded with MoO_3 had a poor viscosity reduction effect. The synergistic effect between the two active components was observed. When the impregnation amount of the two active components increased from 10 to 20 wt%, the viscosity reduction rate did not increase significantly. This indicated that 10 wt% MoO_3–ZrO_2/HZSM-5 had a significant catalytic effect. Further impregnation of active ingredients did not effectively increase the contact between the functional components and the reactants. Therefore, the optimal impregnation of mixed oxides was around 10 wt% (Hosseinpour et al., 2020).

3.2.2. Reaction temperature

As shown in Fig. 8, the viscosity of heavy oil decreased with temperature increasing regardless of whether the catalyst was added. This was because hydrothermal pyrolysis rate increased with the growth of reaction temperature. The reaction rate varied obviously with temperatures between 160 and 240 °C. At 240–320 °C, the reaction tended to be stable. After adding the catalyst, the viscosity reduction rate of heavy oil reached 27.79% at 160 °C. At the same temperature, the viscosity reduction rate was only 13.50% without a catalyst. As the temperature increases, the rate of substance transport for the reaction also increased. At the same time, the temperature increase also accelerated the diffusion of lamellar molecular sieves in heavy oil. This made the reaction more intense. The macromolecular carbon chains in the oil samples unfolded with the temperature increasing. The resistance between molecules was weakened. In addition, sulfur atoms in the reactant frequently contacted the active component in the macroporous structure and formed coordination bonds. At the same time, the increase of strong acid sites in NH_3-TPD accelerated the reaction rates of electron transfer and hydrodesulfurization in hydrothermal cracking reactions. Macroporous and mesoporous structures provided sites for reactions. It was worth noting that when the temperature rose to 280 °C, the viscosity reduction rate of heavy oil would no longer increase significantly.

3.2.3. Catalyst addition

The heavy oil viscosity reduction experiment in Fig. 9 was carried out under 280 °C and 24 h. The addition amounts of catalysts were 0, 0.01, 0.05, 0.5, 1 and 5 wt%, respectively. It could be seen from Fig. 9 that the viscosity reduction rate of oil increased with the increase of catalyst addition. This was because the active metal

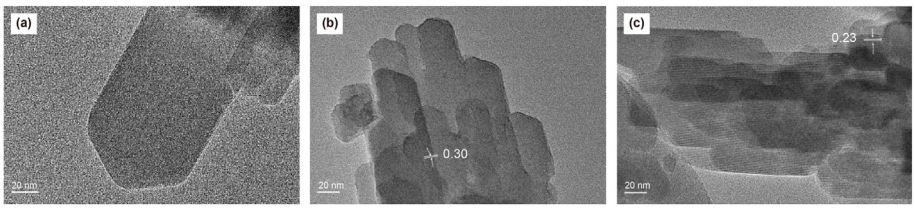

Fig. 5. TEM spectra of different catalysts ((**a**). HZSM-5; (**b**). ZrO_2/HZSM-5; (**c**). MoO_3/HZSM-5).

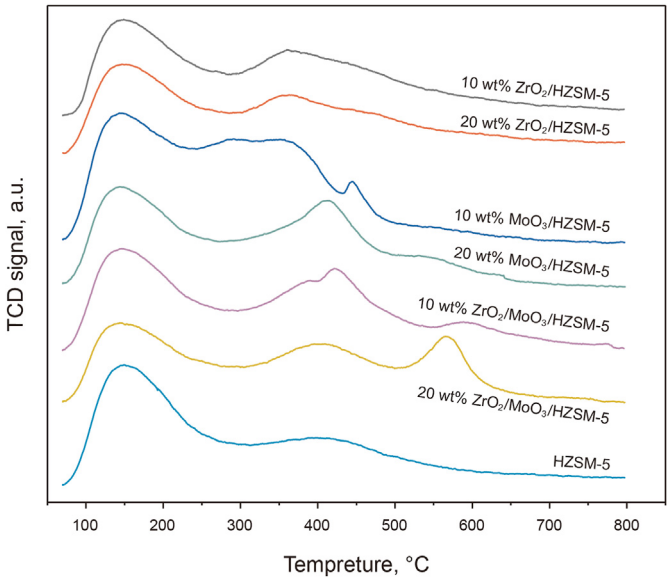

Fig. 6. NH_3 temperature-programmed desorption curve.

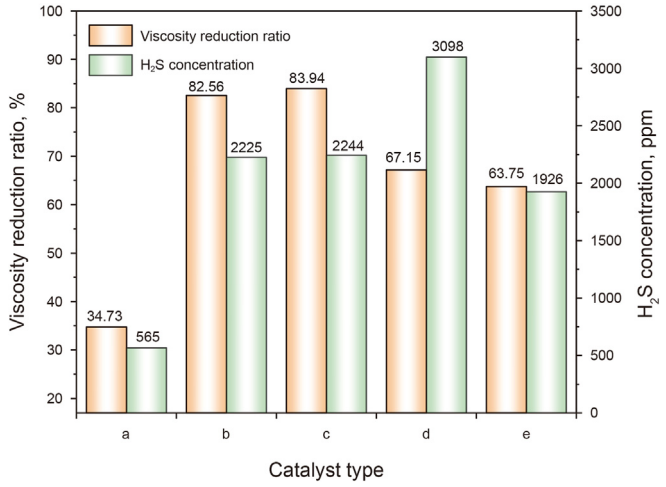

Fig. 7. Effects of catalyst types on viscosity reduction rate and H_2S concentration. a: HZSM-5; b: 10 wt% MoO_3–ZrO_2/HZSM-5; c: 20 wt% MoO_3–ZrO_2/HZSM-5; d: 20 wt% ZrO_2/HZSM-5; e: 20 wt% MoO_3/HZSM-5.

component increased with the catalyst addition increasing. The reaction was facilitated by more active metallic components in contact with the reactants. When the amount of catalyst increased to 1 wt%, the viscosity reduction effect tended to be stable. This was because the reaction reached equilibrium. When the amount of catalyst was 1 wt%, the viscosity reduction rate of the heavy oil sample was 82.26%. When the amount of catalyst was increased four times, the viscosity reduction rate of the oil sample was 83.44%. The viscosity reduction rate only increased by 1.18%. The viscosity reduction rate of heavy oil samples did not increase significantly. In addition, the excessive addition of catalysts could increase the cost of heavy oil recovery. Therefore, the optimal addition amount of catalyst in this experiment was 1 wt%.

3.3. Analysis of oil samples

3.3.1. SARA analysis of oil samples

The changes of SARA compositions of oil samples after reaction are shown in Fig. 10. The resin fraction was significantly reduced. The number of light components increased when the catalyst was added. This indicated that the catalyst promoted the cracking of macromolecules of resins. Therefore, the viscosity reduction of oil reduced. With the increase of temperature and catalyst content, the content of saturated and aromatic fractions increased, and the asphaltene and colloid decreased.

3.3.2. Elemental analysis of oil samples

The elemental analysis results are shown in Table 1. Under the influence of catalysts, the sulfur content element changed significantly. When the catalyst was not added, the sulfur content in the oil sample decreased from 1.34% to 1.15% with the temperature increasing. After adding the catalyst, the sulfur content in the oil sample decreased from 1.29% to 0.88% with the temperature increasing. This indicated that the catalysts could promote the cracking of sulfur-containing substances. The increase of reaction temperature enhanced the degree of hydrothermal cracking reaction. When no catalyst was added, the H/C value increased first and

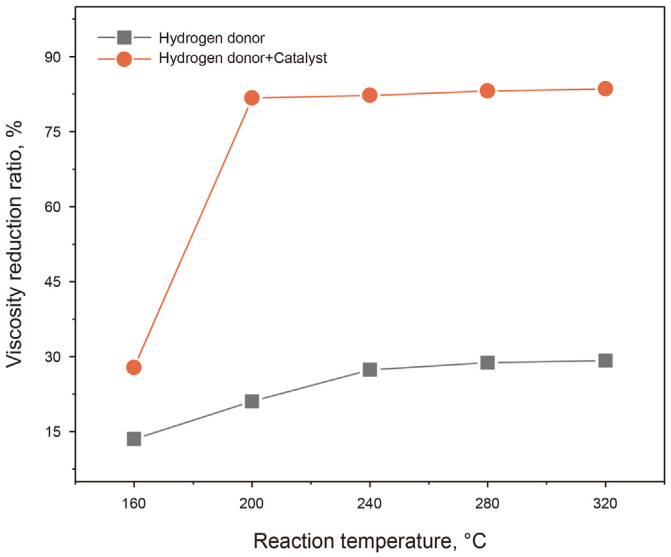

Fig. 8. Effect of temperature on the viscosity reduction rate with or without 10 wt% MoO_3–ZrO_2/HZSM-5.

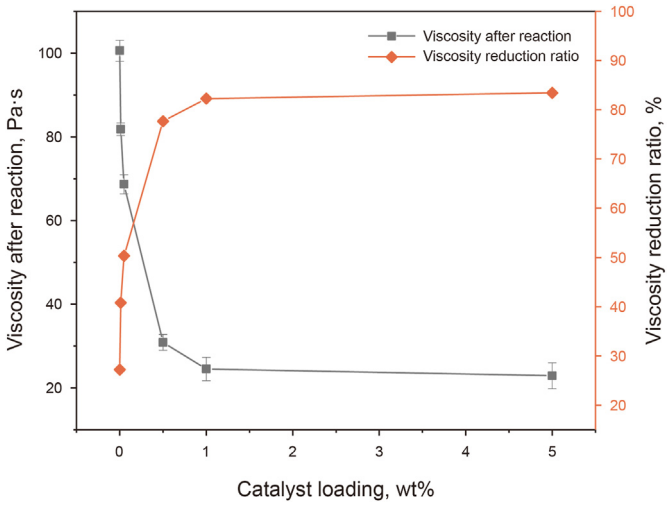

Fig. 9. Effects of different catalyst additions on the viscosity reduction rate.

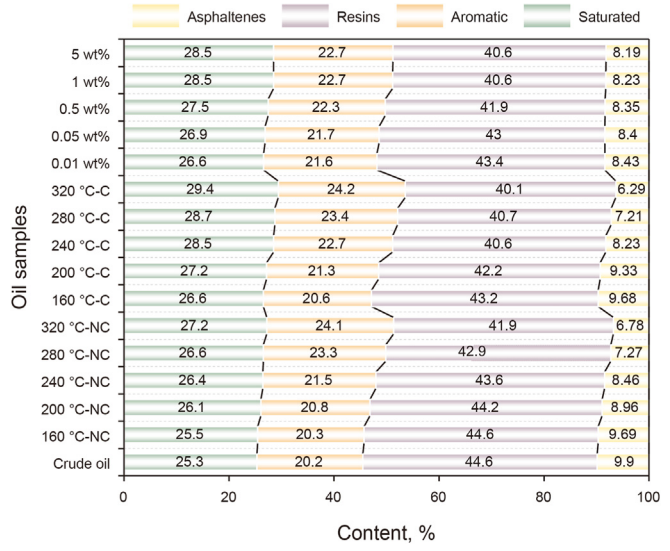

Fig. 10. The changes of SARA compositions of different oil samples. NC: no catalyst added; C: adding catalyst; 1 wt%: the amount of catalyst.

then decreased with increasing temperature. This was because the rate of hydrothermal cracking reaction rate increased with the rise of temperature. However, the asphaltene was cracked into light components and coke. The generation of coke results in the decrease of H/C value in the oil sample. The coke production led to the decline of H/C value in the oil sample.

Compared with the experiment without catalyst, the hydrogenation reaction was more intense after adding catalyst. Therefore, the value of H/C was increased. With the increase of catalyst addition, the sulfur content in the oil sample decreased, and the saturation of carbon atoms increased. The quality of the oil was improved after the reaction. When the amount of catalyst increased from 0.01 to 1 wt%, the sulfur content of oil samples decreased from 1.28% to 1.03%. The H/C value rose from 0.1084 to 0.1127. More free radicals were generated in the reaction. The hydrogen atom could better participate in the hydrogenation reaction. This increased the amount of hydrogen in the oil sample. The catalyst had good surface acidity. This promoted the hydrodesulfurization reaction of alkaline asphaltene. When the amount of catalyst was 1 wt%, the sulfur content of the oil sample decreased to 1.03%. The content of the nitrogen element did not change with the catalyst content increasing. It indicated that the nitrogen element did not participate in the hydrothermal cracking reaction under this condition. The C—N bond has higher bond energy. Therefore, it needs a higher temperature to react violently. This indicated that the catalyst had no noticeable catalytic effect on the denitrification reaction of heavy oil.

3.4. Viscosity reduction mechanism

3.4.1. XPS characterization of oil samples

Fig. 11(a) presented the XPS spectra of the oil sample before reaction. As shown in Fig. 11(a), the peak of S could be seen in the measurement spectrum. Sulfur elements in heavy oil exist in five forms: thioether, thiophene sulfur, sulfoxide sulfur, sulfone sulfur, and sulfate. Their proportions were 12.21%, 24.44%, 12.56%, 34.20% and 16.59%, respectively. There was more unstable sulfone sulfur in the oil sample. It was easy to participate in the reaction and convert to H_2S and other types of stable sulfur.

Fig. 11(b) showed the XPS image of the oil sample after the reaction when the hydrogen donor was added. Compared with that before the reaction, the contents of thioether and sulfone sulfur changed. The content of thioether at 163.69 eV increased from

Table 1
Elementary analysis of oil samples.

Reactant	Temperature, °C	H, %	C, %	N, %	S, %	H/C
Crude oil	/	9.13	86.24	1.11	1.45	0.1059
Hydrogen-only treatment	160	9.44	88.10	1.12	1.34	0.1072
	200	9.47	88.14	1.13	1.27	0.1074
	240	9.52	88.11	1.11	1.27	0.1080
	280	9.57	88.07	1.12	1.24	0.1087
	320	9.56	88.16	1.13	1.15	0.1084
Treatment with catalyst and hydrogen	160	9.71	87.88	1.12	1.29	0.1105
	200	9.84	87.95	1.05	1.16	0.1119
	240	9.92	88.05	1.00	1.03	0.1127
	280	9.97	88.12	0.93	0.98	0.1131
	320	9.99	88.30	0.83	0.88	0.1131
Adding 0.01 wt% catalyst	280	9.55	88.07	1.10	1.28	0.1084
Adding 0.05 wt% catalyst	280	9.63	88.10	1.08	1.19	0.1093
Adding 0.5 wt% catalyst	280	9.71	88.09	1.05	1.15	0.1102
Adding 1 wt% catalyst	280	9.92	88.05	1.00	1.03	0.1127
Adding 5 wt% catalyst	280	9.93	88.05	1.00	1.02	0.1128

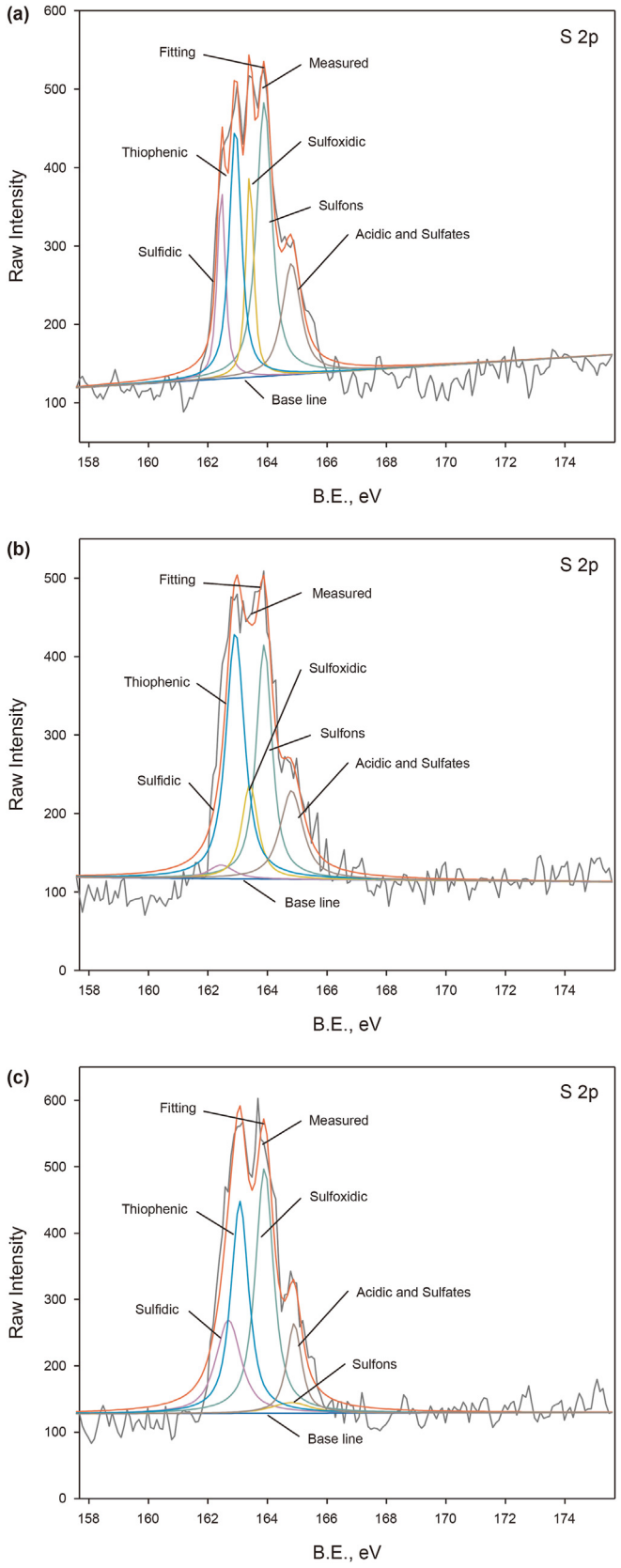

Fig. 11. XPS spectra of oil samples ((**a**). Crude oil; (**b**). Not catalyzed after reaction at 280 °C; (**c**). Catalyzed after reaction at 280 °C).

12.21% to 13.81%. The content of sulfone sulfur at 167.78 eV decreased from 34.20% to 30.41%. In hydrothermal cracking, some unstable thioether and sulfone sulfur were desulfurized. They were converted into more stable thiophene sulfur.

Fig. 11(c) showed the XPS spectra of sulfur in oil samples after reaction with a catalyst added. It showed that the content of unable sulfone sulfur and sulfoxide sulfur in oil decreased after reaction at 280 °C. And the content of relatively stable thioether and thiophene sulfur increased. The content of the sulfur-containing functional group was compared with only hydrogen supply. The content of thioether at 162.58 eV increased from 13.81% to 18.80%. The content of thiophene sulfur at 165.55 eV increased from 24.58% to 30.15%. The sulfoxide sulfur content at 165.55 eV decreased from 12.57% to 10.57%. The sulfone sulfur content at 167.78 eV decreased from 30.41% to 16.27%. The sulfate content at 168.94 eV increased from 18.63% to 24.21%. This indicated that the desulfurization reaction occurred mainly in unstable thioether and sulfone sulfur during the catalytic reaction. The catalyst promoted the transformation of unstable sulfides into more stable thiophene sulfur and hydrogen sulfide gas.

3.4.2. Reaction pathways of sulfone sulfur and sulfoxide sulfur

Fig. 12(a) showed the reaction path of sulfone sulfur hydrothermal pyrolysis. Firstly, the dissociated and adsorbed H_2 formed the B-acid site with the catalyst active center. The two oxygen atoms in sulfone sulfur were absorbed in the L-acid site. B-acid provided hydrogen ions and contributed protons. Then the reaction removed oxygen atoms in the form of water. The C—S bond in sulfone sulfur was broken. Then, they produced small molecule sulfur compounds. Other macromolecules also occurred ring-opening reaction. Fig. 12(b) showed the hydrolysis process of sulfoxide sulfur. The sulfur atom in sulfoxide sulfur was only connected to one oxygen atom. Therefore, it had strong C—S bond energy and good stability. As the temperature increased, sulfoxide sulfur hydrolyzed and released hydrogen sulfide gas.

3.5. Analysis of desulfurization effect of heavy oil

Fig. 13(a) showed the experimental results at different temperatures after adding hydrogen donor and catalyst. The viscosity reduction rate of heavy oil increased with temperature increase. When the temperature reached 200 °C, the viscosity reduction effect of the catalyst tended to be stable. If the reaction temperature continued to rise, the viscosity reduction rate of the catalyst would hardly increase. The catalyst could only break a few chemical bonds at low-temperature. With the temperature increasing, more C—S bonds were broken in heavy oil. Therefore, when the temperature reached 200 °C or higher, the viscosity reduction rate of heavy oil was improved. The yield of hydrogen sulfide was also increased.

It could be seen from Fig. 13(b) that when the amount of catalyst was fewer, the viscosity reduction rate increased with the catalyst increasing. When the amount of catalyst reached 1 wt%, the viscosity reduction effect tended to be stable. If the amount of catalyst continued to increase, the viscosity reduction rate of the heavy oil would hardly increase. When the amount of catalyst was fewer, it could only interact with a small amount of colloid and asphaltene. Its stable structure cannot be completely broken. With the catalyst dosage increasing, the planar stacking structure of asphaltene was destroyed. The viscosity reduction rate of heavy oil increased significantly. Considering the economy and viscosity reduction effect of heavy oil, the optimal dosage of catalyst was 1 wt%.

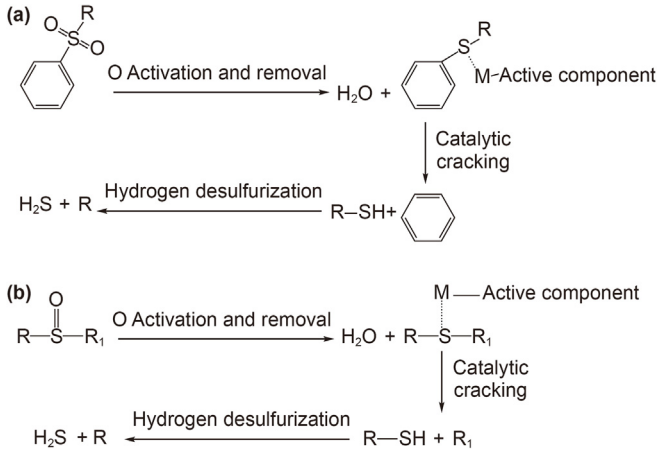

Fig. 12. Hydrothermal cracking reaction path ((**a**). Sulfone sulfur; (**b**). Sulfoxide sulfur).

3.6. Economical analysis

Table 2 evaluated the cost of catalyst preparation using 10 wt% MoO_3–ZrO_2/HZSM-5 as an example. The catalyst preparation cost mainly includes raw material, utility and capital costs (Ong et al., 2022). The raw material cost is mainly the purchase cost of raw materials in the catalyst preparation process. The utility cost primarily considers the total energy consumed in the catalyst preparation process (e.g., drying, ultrasonic shaking, calcination, etc.). Capital cost is the capital cost of the experimental equipment required in the catalyst preparation process. Among them, the equipment is the original fixed assets of the laboratory. The total cost of raw materials and utilities of the 10 wt% MoO_3–ZrO_2/HZSM-5 catalyst with the best viscosity reduction was $6.7618/kg.

In the Gudong Oil Production Plant field experiment, the amounts of steam and catalyst injected were 1300 tons and 6.5 tons, respectively (Qin et al., 2009). The crude oil recovery was increased by 21.07% with the addition of 0.005 wt% SiO_2 nanocatalyst (Song, 2023). Therefore, 0.005 wt% catalyst will be added into 1 ton of steam. The field test showed that the oil-to-steam ratio increased by 0.24 after adding catalyst, resulting in an additional net gain of $171,460 (Xu et al., 1998). When every 1000 tons of steam is injected, 5 tons catalyst is required. The additional oil production is 240 tons. The cost of the catalyst is $33,809. The benefit of additional oil recovery is $91,440. Therefore, this is economically feasible.

Table 2
Catalyst preparation cost.

Cost items	Component	Unit price	Cost of catalyst
Raw material cost	$Zr(NO_3)_4 \cdot 5H_2O$	$0.1010/kg	$0.0340/kg
	$(NH_4)_2MoO_4$	$0.1948/kg	$0.0133/kg
	HZSM-5	$6.4935/kg	$4.9188/kg
Utility cost	Electricity expense	$0.0519/kWh	$1.7957/kg
Capital cost	Ultrasonic oscillator	$315.91	$315.91
	Oven	$376.07	$376.07
	Muffle furnace	$558.22	$558.22

4. Conclusion

HZSM-5, MoO_3/HZSM-5, ZrO_2/HZSM-5 and MoO_3–ZrO_2/HZSM-5 catalysts were developed to promote desulfurization and viscosity reduction of heavy oil. The effects of temperature, catalyst type and addition amount on the viscosity and composition of oil were evaluated. The main conclusions are listed below.

(1) The prepared catalysts are uniformly loaded with active components and have good spatial structure and catalytic activity. The catalysts have economic feasibility and application potential.
(2) The result showed that the optimal addition amount of MoO_3–ZrO_2/HZSM-5 catalyst was 1 wt%. The optimal reaction temperature was 280 °C. The optimum impregnation of the catalyst active component was 10 wt%. The mass ratio of the two active ingredients was 1:1. Under these conditions, the viscosity reduction rate of heavy oil reached 82.26%.
(3) SARA result showed that the contents of resins and asphaltic in the oil after the catalytic reaction was 5.69%. It is lower than that in crude oil. The H/C value of the oil sample increased from 0.1059 to 0.1126. Meanwhile, sulfur content decreased from 1.45% to 1.03%. This was because part of sulfur existed in H_2S gas after the reaction.
(4) The sulfur element distribution of oil samples before and after the reaction was analyzed by XPS. The results showed that the sulfoxide and sulfone sulfur content in the oil samples decreased by 19.92%. The content of stable thiophene sulfur increased by 5.71%.

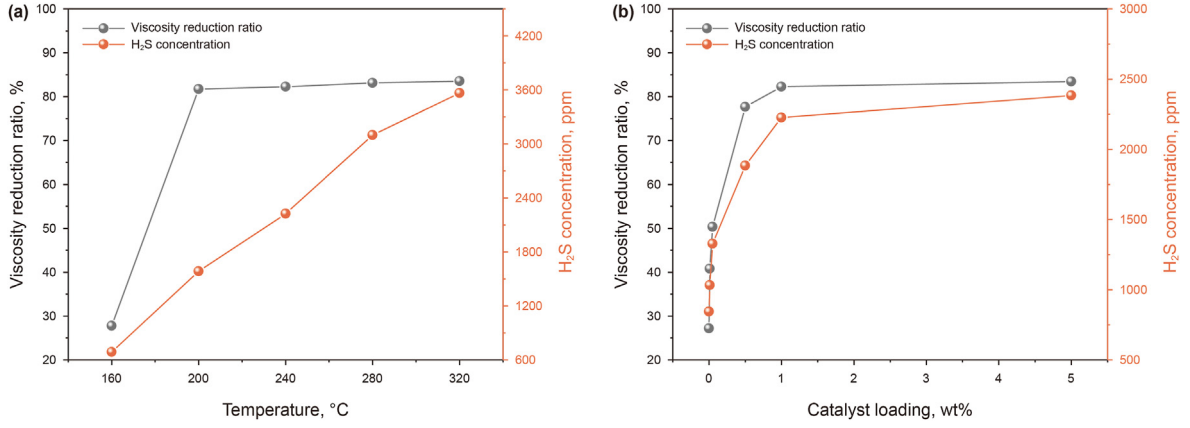

Fig. 13. Effect of temperature/catalyst addition on viscosity reduction and desulfurization of heavy oil ((**a**). Temperature; (**b**). Catalyst addition).

Declaration of interests

The authors declare that they have no known competing financial interests or personal relationships that could have appeared to influence the work reported in this paper.

Acknowledgements

The authors would like to acknowledge the financial support provided by the National Science and Technology Major Project of the Ministry of Science and Technology of China (2016ZX05012-002-005), Shandong Provincial Natural Science Foundation (Grant no.: ZR2021QE051), National Natural Science Foundation of China (Grant no.: 52206291), and the Fundamental Research Funds for the Central Universities (Grant no.: 22CX06030A).

References

Aghaei, E., Haghighi, M., 2014. High temperature synthesis of nanostructured Ce-SAPO-34 catalyst used in conversion of methanol to light olefins: effect of temperature on physicochemical properties and catalytic performance. J. Porous Mater. 22, 187–200. https://doi.org/10.1007/s10934-014-9885-5.

Al-Attas, T.A., Zahir, M.H., Ali, S.A., et al., 2019. Kinetics of the synergy effects in heavy oil upgrading using novel Ni-p-tert-butylcalix[4]arene as a dispersed catalyst with a supported catalyst. Fuel Process. Technol. 185, 158–168. https://doi.org/10.1016/j.fuproc.2018.12.003.

Antwi Peprah, B., Brown, O., Stryker, J.M., et al., 2020. Sulfided homogeneous iron precatalyst for partial hydrogenation and hydrodesulfurization of polycyclic aromatic model asphaltenes. Energy Fuels 34, 16532–16541. https://doi.org/10.1021/acs.energyfuels.0c02908.

Antwi Peprah, B., Brown, O., Stryker, J.M., et al., 2023. Selective hydrogenation and defunctionalization of heavy oil model compounds using an unsupported iron catalyst. Fuel 333, 126184. https://doi.org/10.1016/j.fuel.2022.126184.

Avbenake, O.P., Al-Hajri, R.S., Jibril, B.Y., 2019. Catalytic upgrading of heavy oil using NiCo/γ-Al_2O_3 catalyst: effect of initial atmosphere and water-gas shift reaction. Fuel 235, 736–743. https://doi.org/10.1016/j.fuel.2018.08.074.

Baharudin, K.B., Taufiq-Yap, Y.H., Hunns, J., et al., 2019. Mesoporous NiO/Al-SBA-15 catalysts for solvent-free deoxygenation of palm fatty acid distillate. Microporous Mesoporous Mater. 276, 13–22. https://doi.org/10.1016/j.micromeso.2018.09.014.

Bandara, J., Kuruppu, S.S., Pradeep, U.W., 2006. The promoting effect of MgO layer in sensitized photodegradation of colorants on TiO_2/MgO composite oxide. Colloids Surf. A Physicochem. Eng. Asp. 276, 197–202. https://doi.org/10.1016/j.colsurfa.2005.10.059.

Chen, Y.L., Wang, Y.Q., Lu, J.Y., et al., 2009a. The viscosity reduction of nano-keggin-$K_3PMo_{12}O_{40}$ in catalytic aquathermolysis of heavy oil. Fuel 88, 1426–1434. https://doi.org/10.1016/j.fuel.2009.03.011.

Chen, Y.M., Xiao, B., Chang, J., et al., 2009b. Synthesis of biodiesel from waste cooking oil using immobilized lipase in fixed bed reactor. Energy Convers. Manag. 50, 668–673. https://doi.org/10.1016/j.enconman.2008.10.011.

Clark, P.D., Kirk, M.J., 1994. Studies on the upgrading of bituminous oils with water and transition metal catalysts. Energy Fuels 8, 380–387. https://doi.org/10.1021/ef00044a014.

Clark, P.D., Lesage, K.L., Tsang, G.T., et al., 1988. Reactions of benzo[b] thiophene with aqueous metal species: their influence on the production and processing of heavy oils. Energy Fuels 2, 578–581. https://doi.org/10.1021/ef00010a027.

Cui, J.J., Zhang, Z.H., Liu, X.D., et al., 2020. Analysis of the viscosity reduction of crude oil with nano-Ni catalyst by acoustic cavitation. Fuel 275, 117976. https://doi.org/10.1016/j.fuel.2020.117976.

de Klerk, A., 2021. Processing unconventional oil: partial upgrading of oilsands bitumen. Energy Fuels 35, 14343–14360. https://doi.org/10.1021/acs.energyfuels.1c02128.

Dong, J., Xu, Z., Kuznicki, S.M., 2009. Magnetic multi-functional nano composites for environmental applications. Adv. Funct. Mater. 19, 1268–1275. https://doi.org/10.1002/adfm.200800982.

Dutta, R.P., Mccaffrey, W.C., Gray, M.R., 2000. Thermal cracking of athabasca bitumen: influence of steam on reaction chemistry. Energy Fuels 14, 671–676. https://doi.org/10.1021/ef990223e.

Ghanavati, M., Shojaei, M.J., SaadatAbadi, A.R., 2013. Effects of asphaltene content and temperature on viscosity of iranian heavy crude oil: experimental and modeling study. Energy Fuels 27, 7217–7232. https://doi.org/10.1021/ef400776h.

Ghanbari, B., Zangeneh, F.K., Rizi, Z.T., et al., 2018. Highly efficient production of benzene-free aromatics from methanol over low-Si/Al-ratio alkali-modified Fe/Zn/HZSM-5. ACS Omega 3, 18821–18835. https://doi.org/10.1021/acsomega.8b01380.

Groenzin, H., Mullins, O.C., 2000. Molecular size and structure of asphaltenes from various sources. Energy Fuels 14, 677–684. https://doi.org/10.1021/ef990225z.

Hart, A., 2013. A review of technologies for transporting heavy crude oil and bitumen via pipelines. J. Pet. Explor. Prod. Technol. 4, 327–336. https://doi.org/10.1007/s13202-013-0086-6.

Hart, A., Lewis, C., White, T., et al., 2015. Effect of cyclohexane as hydrogen-donor in ultradispersed catalytic upgrading of heavy oil. Fuel Process. Technol. 138, 724–733. https://doi.org/10.1016/j.fuproc.2015.07.016.

Hashemi, R., Nassar, N.N., Pereira Almao, P., 2013. Enhanced heavy oil recovery by in situ prepared ultradispersed multimetallic nanoparticles: a study of hot fluid flooding for athabasca bitumen recovery. Energy Fuels 27, 2194–2201. https://doi.org/10.1021/ef3020537.

Headen, T.F., Boek, E.S., Jackson, G., et al., 2017. Simulation of asphaltene aggregation through molecular dynamics: insights and limitations. Energy Fuels 31, 1108–1125. https://doi.org/10.1021/acs.energyfuels.6b02161.

Hendraningrat, L., Torsæter, O., 2014. Metal oxide-based nanoparticles: revealing their potential to enhance oil recovery in different wettability systems. Appl. Nanosci. 5, 181–199. https://doi.org/10.1007/s13204-014-0305-6.

Hofko, B., Eberhardsteiner, L., Füssl, J., et al., 2015. Impact of maltene and asphaltene fraction on mechanical behavior and microstructure of bitumen. Mater. Struct. 49, 829–841. https://doi.org/10.1617/s11527-015-0541-6.

Hosseinpour, M., Soltani, M., Noofeli, A., et al., 2020. An optimization study on heavy oil upgrading in supercritical water through the response surface methodology (RSM). Fuel 271, 117618. https://doi.org/10.1016/j.fuel.2020.117618.

Hu, S.J., Zhu, J.H., Wu, B.C., et al., 2020. Green synthesis of ester base oil with high viscosity – part I: catalyst preparation, characterization, evaluation, and mechanism analysis. Fuel 274, 117802. https://doi.org/10.1016/j.fuel.2020.117802.

Jong, K.P., Zecevic, J., Friedrich, H., et al., 2010. Zeolite Y crystals with trimodal porosity as ideal hydrocracking catalysts. Angew. Chem. Int. Ed. 49, 10074–10078. https://doi.org/10.1002/anie.201004360.

Kordulis, C., Bourikas, K., Gousi, M., et al., 2016. Development of nickel based catalysts for the transformation of natural triglycerides and related compounds into green diesel: a critical review. Appl. Catal. B Environ. 181, 156–196. https://doi.org/10.1016/j.apcatb.2015.07.042.

Lakhova, A., Petrov, S., Ibragimova, D., et al., 2017. Aquathermolysis of heavy oil using nano oxides of metals. J. Petrol. Sci. Eng. 153, 385–390. https://doi.org/10.1016/j.petrol.2017.02.015.

Laredo, G.C., López, C.R., Álvarez, R.E., et al., 2004. Naphthenic acids, total acid number and sulfur content profile characterization in Isthmus and Maya crude oils. Fuel 83, 1689–1695. https://doi.org/10.1016/j.fuel.2004.02.004.

Li, C., Zhang, C., Gholizadeh, M., et al., 2020. Different reaction behaviours of light or heavy density polyethylene during the pyrolysis with biochar as the catalyst. J. Hazard Mater. 399, 123075. https://doi.org/10.1016/j.jhazmat.2020.123075.

Li, G.R., Chen, Y., An, Y., et al., 2016. Catalytic aquathermolysis of super-heavy oil: cleavage of CS bonds and separation of light organosulfurs. Fuel Process. Technol. 153, 94–100. https://doi.org/10.1016/j.fuproc.2016.06.007.

Li, H.W., Ma, H.W., Zhao, W.J., et al., 2019a. Upgrading lignin bio-oil for oxygen-containing fuel production using Ni/MgO: effect of the catalyst calcination temperature. Appl. Energy 253, 113613. https://doi.org/10.1016/j.apenergy.2019.113613.

Li, H.Y., Gao, H., Zhao, X.N., et al., 2022. Experimental study on viscosity reduction of heavy oil with water content by synergistic effect of microwave and nano-catalyst. J. Petrol. Sci. Eng. 208, 109271. https://doi.org/10.1016/j.petrol.2021.109271.

Li, J.J., Zhou, T.D., Tang, X.D., et al., 2019b. Viscosity reduction process of heavy oil by catalytic co-pyrolysis with sawdust. J. Anal. Appl. Pyrol. 140, 444–451. https://doi.org/10.1016/j.jaap.2019.04.027.

Li, W.L., Zheng, J.Y., Luo, Y.B., et al., 2017. Hierarchical zeolite Y with full crystallinity: formation mechanism and catalytic cracking performance. Energy Fuels 31, 3804–3811. https://doi.org/10.1021/acs.energyfuels.6b03421.

Lin, D., Zhu, H.H., Wu, Y.N., et al., 2019. Morphological insights into the catalytic aquathermolysis of crude oil with an easily prepared high-efficiency Fe_3O_4-containing catalyst. Fuel 245, 420–428. https://doi.org/10.1016/j.fuel.2019.02.063.

Lin, R., Chen, K., Miao, M.Q., et al., 2020. Reaction mechanism of H_2S generation during tetrahydrothiophene aquathermolysis reaction. Energy Fuels 34, 2781–2789. https://doi.org/10.1021/acs.energyfuels.9b03844.

Liu, B., Zhao, K.D., Chai, Y.M., et al., 2019. Slurry phase hydrocracking of vacuum residue in the presence of presulfided oil-soluble MoS_2 catalyst. Fuel 246, 133–140. https://doi.org/10.1016/j.fuel.2019.02.114.

Liu, D., Tang, J.S., Zheng, R.N., et al., 2020. Influence of steam on the coking characteristics of heavy oil during in situ combustion. Fuel 264, 116904. https://doi.org/10.1016/j.fuel.2019.116904.

Lv, X.B., Fan, W.Y., Wang, Q.T., et al., 2019. Synthesis, characterization, and mechanism of copolymer viscosity reducer for heavy oil. Energy Fuels 33, 4053–4061. https://doi.org/10.1021/acs.energyfuels.9b00217.

Montoya, T., Argel, B.L., Nassar, N.N., et al., 2016. Kinetics and mechanisms of the catalytic thermal cracking of asphaltenes adsorbed on supported nanoparticles. Petrol. Sci. 13, 561–571. https://doi.org/10.1007/s12182-016-0100-y.

Muley, P.D., Henkel, C., Abdollahi, K.K., et al., 2015. Pyrolysis and catalytic upgrading of pinewood sawdust using an induction heating reactor. Energy Fuels 29, 7375–7385. https://doi.org/10.1021/acs.energyfuels.5b01878.

Mullins, O.C., 2010. The modified yen model. Energy Fuels 24, 2179–2207. https://doi.org/10.1021/ef900975e.

Muraza, O., Galadima, A., 2015. Aquathermolysis of heavy oil: a review and perspective on catalyst development. Fuel 157, 219–231. https://doi.org/10.1016/j.fuel.2015.04.065.

Nguyen, N., Chen, Z.X., Pereira Almao, P., et al., 2017. Reservoir simulation and production optimization of bitumen/heavy oil via nanocatalytic in situ upgrading. Ind. Eng. Chem. Res. 56, 14214–14230. https://doi.org/10.1021/acs.iecr.7b03819.

Oh, S., Lee, J.H., Choi, I.G., et al., 2020. Enhancement of bio-oil hydrodeoxygenation activity over Ni-based bimetallic catalysts supported on SBA-15. Renew. Energy 149, 1–10. https://doi.org/10.1016/j.renene.2019.12.027.

Olvera, J.N.R., Gutiérrez, G.J., Serrano, J.A.R., et al., 2014. Use of unsupported, mechanically alloyed NiWMoC nanocatalyst to reduce the viscosity of aquathermolysis reaction of heavy oil. Catal. Commun. 43, 131–135. https://doi.org/10.1016/j.catcom.2013.09.027.

Ong, J.L., Loy, A.C.M., Teng, S.Y., et al., 2022. Future paradigm of 3D printed Ni-based metal organic framework catalysts for dry methane reforming: techno-economic and environmental analyses. ACS Omega 7, 15369–15384. https://doi.org/10.1021/acsomega.1c06873.

Parejas, R.D.L.C., Moura, F.J., Avillez, R.R.D., et al., 2021. Effects of Al_2O_3-NiO, TiO_2 and (Mg, Ni)O particles on the viscosity of heavy oil during aquathermolysis. Colloids Surf. A Physicochem. Eng. Asp. 625, 126863. https://doi.org/10.1016/j.colsurfa.2021.126863.

Qin, W.L., Sun, B.Y., Pu, C.S., 2009. Application of high-efficiency catalysts in thick oil downhole reforming and viscosity reduction extraction. Acta Pet. Sin. 25, 772–776 (in Chinese).

Qiu, Z.Z., Zhai, Y.B., Li, S.H., et al., 2020. Catalytic co-pyrolysis of sewage sludge and rice husk over biochar catalyst: bio-oil upgrading and catalytic mechanism. Waste Manag. 114, 225–233. https://doi.org/10.1016/j.wasman.2020.07.013.

Safaei Mahmoudabadi, Z., Rashidi, A., Panahi, M., 2021. New approach to unsupported ReS_2 nanorod catalyst for upgrading of heavy crude oil using methane as hydrogen source. Int. J. Hydrogen Energy 46, 5270–5285. https://doi.org/10.1016/j.ijhydene.2020.11.077.

Schuler, B., Meyer, G., Pena, D., et al., 2015. Unraveling the molecular structures of asphaltenes by atomic force microscopy. J. Am. Chem. Soc. 137, 9870–9876. https://doi.org/10.1021/jacs.5b04056.

Sitnov, S.A., Mukhamatdinov, I.I., Vakhin, A.V., et al., 2018. Composition of aquathermolysis catalysts forming in situ from oil-soluble catalyst precursor mixtures. J. Petrol. Sci. Eng. 169, 44–50. https://doi.org/10.1016/j.petrol.2018.05.050.

Song, Q., 2023. An indoor study on the modification of core wettability and recovery enhancement by nano-SiO_2 particles. Adv. Fine Petrochem. 24, 6–9. https://doi.org/10.13534/j.cnki.32-1601/te.2023.01.002 (in Chinese).

Suwaid, M.A., Varfolomeev, M.A., Al-muntaser, A.A., et al., 2020. In-situ catalytic upgrading of heavy oil using oil-soluble transition metal-based catalysts. Fuel 281, 118753. https://doi.org/10.1016/j.fuel.2020.118753.

Sviridenko, N.N., Golovko, A.K., Kirik, N.P., et al., 2020. Upgrading of heavy crude oil by thermal and catalytic cracking in the presence of NiCr/WC catalyst. J. Taiwan Inst. Chem. Eng. 112, 97–105. https://doi.org/10.1016/j.jtice.2020.06.018.

Taborda, E.A., Franco, C.A., Ruiz, M.A., et al., 2017. Experimental and theoretical study of viscosity reduction in heavy crude oils by addition of nanoparticles. Energy Fuels 31, 1329–1338. https://doi.org/10.1021/acs.energyfuels.6b02686.

Tran, Q.K., Han, S.J., Ly, H.V., et al., 2020. Hydrodeoxygenation of a bio-oil model compound derived from woody biomass using spray-pyrolysis-derived spherical γ-Al_2O_3-SiO_2 catalysts. J. Ind. Eng. Chem. 92, 243–251. https://doi.org/10.1016/j.jiec.2020.09.012.

Wang, H., Wu, Y., He, L., et al., 2012. Supporting tungsten oxide on zirconia by hydrothermal and impregnation methods and its use as a catalyst to reduce the viscosity of heavy crude oil. Energy Fuels 26, 6518–6527. https://doi.org/10.1021/ef301064b.

Wang, J., Tang, X., Li, J., et al., 2021. Quartz sand proppant loaded with Ni and Mo for in-situ aquathermolysis of heavy oil. Fuel 306, 121653. https://doi.org/10.1016/j.fuel.2021.121653.

Wei, X.C., Xue, X.F., Wu, L., et al., 2020. High-grade bio-oil produced from coconut shell: a comparative study of microwave reactor and core-shell catalyst. Energy 212, 118692. https://doi.org/10.1016/j.energy.2020.118692.

Weissman, J.G., 1997. Review of processes for downhole catalytic upgrading of heavy crude oil. Fuel Process. Technol. 50, 199–213. https://doi.org/10.1016/s0378-3820(96)01067-3.

Xu, J., Zhang, Q., Wu, F., et al., 1998. Field steam throughput test of thick oil thermal recovery additives. J. Xi'an Shiyou Univ. (Nat. Sci. Ed.) 6, 31–33 (in Chinese).

Yang, T.F., Liu, C.C., Li, C., et al., 2020. Promotion effect with dispersed Fe-Ni-S catalyst to facilitate hydrogenolysis of lignite and heavy residue. Fuel 259, 116303. https://doi.org/10.1016/j.fuel.2019.116303.

Yenumala, S.R., Kumar, P., Maity, S.K., et al., 2020. Hydrodeoxygenation of karanja oil using ordered mesoporous nickel-alumina composite catalysts. Catal. Today 348, 45–54. https://doi.org/10.1016/j.cattod.2019.08.040.

Zaykovskaya, A.O., Kumar, N., Kholkina, E.A., et al., 2020. Synthesis and physicochemical characterization of Beta zeolite catalysts: evaluation of catalytic properties in Prins cyclization of (−)-isopulegol. Microporous Mesoporous Mater. 302, 110236. https://doi.org/10.1016/j.micromeso.2020.110236.

Zhang, Y., Monnier, J., Ikura, M., 2020. Bio-oil upgrading using dispersed unsupported MoS_2 catalyst. Fuel Process. Technol. 206, 106403. https://doi.org/10.1016/j.fuproc.2020.106403.

Zhang, Y.S., Owen, R.E., Shearing, P.R., et al., 2019. A study of coke formed by heavy oil volatilization/decomposition on Y-zeolite. J. Anal. Appl. Pyrol. 141, 104630. https://doi.org/10.1016/j.jaap.2019.104630.

Zhao, H., Memon, A., Gao, J., et al., 2016. Heavy oil viscosity measurements: best practices and guidelines. Energy Fuels 30, 5277–5290. https://doi.org/10.1021/acs.energyfuels.6b00300.